HHS Public Access

Author manuscript

Biofabrication. Author manuscript; available in PMC 2021 June 12.

Published in final edited form as:

Biofabrication. ; 12(3): 035020. doi:10.1088/1758-5090/ab906e.

3D printed composite scaffolds with dual small molecule delivery for mandibular bone regeneration

Wenhai Zhang[1,2,3], **Wen Shi**[2,3], **Shaohua Wu**[2,3,4], **Mitchell Kuss**[2,3], **Xiping Jiang**[2,5], **Jason B Untrauer**[6], **St Patrick Reid**[7], **Bin Duan**[2,3,8,9,*]

[1]First Hip Department of Orthopedics, Tianjin Hospital, Tianjin, 300211, China

[2]Mary & Dick Holland Regenerative Medicine Program, University of Nebraska Medical Center, Omaha, NE, USA

[3]Division of Cardiology, Department of Internal Medicine, University of Nebraska Medical Center, Omaha, NE, USA

[4]College of Textiles & Clothing; Collaborative Innovation Center of Marine Biomass Fibers, Qingdao University, Qingdao, China

[5]College of Medicine, Department of Genetics, Cell Biology and Anatomy, University of Nebraska Medical Center, Omaha, NE, USA

[6]Division of Oral & Maxillofacial Surgery, Department of Surgery, College of Medicine, University of Nebraska Medical Center, Omaha, NE

[7]College of Medicine, Department of Pathology and Microbiology, University of Nebraska Medical Center, Omaha, NE, USA

[8]Department of Surgery, University of Nebraska Medical Center, Omaha, NE, USA

[9]Department of Mechanical and Materials Engineering, University of Nebraska- Lincoln, Lincoln, NE, USA

Abstract

Functional reconstruction of craniomaxillofacial defects is challenging, especially for the patients who suffer from traumatic injury, cranioplasty, and oncologic surgery. Three-dimensional (3D) printing/bioprinting technologies provide a promising tool to fabricate bone tissue engineering constructs with complex architectures and bioactive components. In this study, we implemented multi-material 3D printing to fabricate 3D printed PCL/hydrogel composite scaffolds loaded with dual bioactive small molecules (i.e. resveratrol and strontium ranelate). The incorporated small molecules are expected to target several types of bone cells. We systematically studied the scaffold morphologies and small molecule release profiles. We then investigated the effects of the released small molecules from the drug loaded scaffolds on the behavior and differentiation of mesenchymal stem cells (MSCs), monocyte-derived osteoclasts, and endothelial cells. The 3D printed scaffolds, with and without small molecules, were further implanted into a rat model with a critical-sized mandibular bone defect. We found that the bone scaffolds containing the dual small

*Corresponding authors: bin.duan@unmc.edu Tel: +1 402 559 9637.

molecules had combinational advantages in enhancing angiogenesis and inhibiting osteoclast activities, and they synergistically promoted MSC osteogenic differentiation. The dual drug loaded scaffolds also significantly promoted *in vivo* mandibular bone formation after 8-week implantation. This work presents a 3D printing strategy to fabricate engineered bone constructs, which can likely be used as off-the-shelf products to promote craniomaxillofacial regeneration.

Graphical Abstract

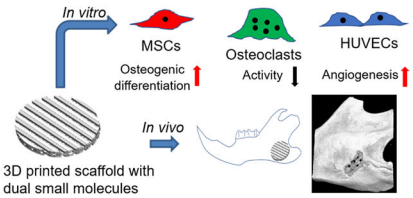

Keywords

Tissue engineering; Vascularization; Craniomaxillofacial reconstruction; Osteogenesis

1. Introduction

Craniomaxillofacial bone defects are common and result from trauma, tumor, bone infection, or hereditary malformation [1]. Repair and regeneration of craniofacial bone defects are challenging due to the complexity of the structures involved and the sophisticated biomechanical and physiological environment [2, 3]. Current approaches for the reconstruction of craniomaxillofacial bone defects include the utilization of autografts and allografts, rigid fixation, and free tissue transfer [4]. However, these strategies are associated with many drawbacks, such as nonunion, plate extrusion, limited availability, donor site morbidity, potential immunogenic rejection, and disease transmission [5, 6]. As an exciting alternative strategy, bone tissue engineering provides novel treatment modalities for craniomaxillofacial bone defect repair and reconstruction [7, 8].

3D printing/bioprinting technologies have been widely used for fabricating engineered bone tissues with complex architectures and customized shapes in a layer-by-layer manner [9, 10]. It is thus a promising technique to accurately replicate the 3D complexity and achieve shape fidelity for surgical reconstruction and regeneration of craniomaxillofacial tissue [11, 12]. By optimizing the pore size and controlling the 3D printed scaffold microstructure, vascularization, and bone regeneration can be improved [13, 14]. However, in most cases, 3D printed scaffolds alone are not osteoinductive in nature. To address this shortcoming, stem cells, especially mesenchymal stem cells (MSCs), and growth factors are incorporated by using various strategies to promote defect regeneration [15, 16]. The autologous cells have osteogenic potential, but they require extensive isolation, manipulation, and culture processing [17]. The use of growth factors (e.g. bone morphogenic protein-2 (BMP-2) and vascular endothelial growth factor (VEGF)) can significantly improve the osteogenesis and vascularization [18]. 3D printing also enables the incorporation of multiple growth factors/peptides to generate heterogeneous tissue constructs and achieve multiple functions [19, 20]. However, several potential complications and concerns are associated with the growth factor

approach, including short half-life, protein instability, undesired dose-related side effects, and higher costs [21]. Small molecules, on the other hand, usually have relatively simple structures, are easy to prepare with less cost, and have a variety of biological functions and applications [22]. Small molecules of both natural and synthetic origin are promising alternatives to biological factors [21].

Resveratrol (RSV) is a polyphenolic phytoalexin, and is regularly obtained from various plants and fruits [23]. It has been demonstrated that RSV has various pharmacological activities, including anti-inflammation [24], antioxidation [25], anticancer [26], and cardiovascular protection [27]. Importantly, RSV can significantly promote bone formation by facilitating osteogenic differentiation and the release of angiogenic factors [28, 29]. Strontium ranelate (SrRn), a strontium (II) salt of ranelic acid, is another small molecule that can increase bone formation and reduces bone resorption [30]. It has dual effects on bone remodeling, with stimulation of osteogenesis and inhibition of osteoclastogenesis [31]. To maximize bone formation, the engineered bone scaffolds are loaded with multiple bioactive small molecules in order to achieve controlled release and targeting of different cell types in the bone tissues.

In the present study, we 3D printed scaffolds consisting of a polycaprolactone/ β-tricalcium phosphate (PCL/TCP) mixture and hydrogel based bioink loaded with RSV, SrRn, or a combination of both. Subsequently, we systematically investigated the effects of drug loaded scaffolds and the released small molecules on the behavior and differentiation of various types of bone cells. We then implanted the scaffolds into a rat model with a critical-sized mandibular bone defect and evaluated *in vivo* bone formation.

2. Materials and methods

2.1 Generation of 3D printed scaffolds

3D printed scaffolds were fabricated using a high-resolution 3D bioprinter (3D-Bioplotter® Manufacturer Series, EnvisionTEC; Dearborn, MI), similarly to our previous method [32]. Briefly, PCL (Mw 80,000, Sigma-Aldrich) and TCP (nanocrystals, mean size 100 nm, Berkeley Advanced Biomaterials, Inc.) (1:2 w/w) were dissolved and suspended in a mixed solvent consisting of dichloromethane (DCM, Acros Organics), dimethylformamide (DMF, Acros Organics), and tetrahydrofuran (THF, Fisher Scientific) (1:1:1 v/v/v) and formed a slurry for the 3D printing of the PCL/TCP frames in each layer throughout the construct. Another printing head deposited methacrylated hyaluronic acid (Me-HA, ~1,200 kDa, NovaMatrix) and methacrylated gelatin (Me-Gel, from type B gelatin, Sigma-Aldrich)-based hydrogels between the PCL/TCP frames [33, 34], as shown in Fig. 1A. The size of the 3D printed scaffolds was 20 mm × 20 mm × 1 mm (L×W×H). For the incorporation of the small molecules, RVS (TCI, 1.0 mg/ml) was dissolved in the mixed solvent together with PCL/TCP, and SrRn (Sigma-Aldrich, 1.0 mg/ml) was added to the Me-HA/Me-Gel hydrogel. Therefore, four types of scaffolds were 3D printed, i.e. scaffold only, scaffold with RVS, scaffold with SrRn, and scaffold with both RVS and SrRn, denoted as Scaffold only, RVS, SrRn, and RVS+SrRn, respectively. The 3D printed scaffolds were dried after printing and then punched into small discs using biopsy punches and were UV sterilized for 2 h (⌀ = 6 mm for *in vitro* characterization and cell culture; ⌀ = 3.5 mm for *in vivo* implantation).

2.2 Morphological characterization and release behaviors of small molecules

The scaffolds were examined via a scanning electron microscope (SEM, FEI Quanta 200) for morphological assessment. Prior to obtaining the SEM images, a thin layer of gold was sputter-coated onto the material samples. For the evaluation of the small molecule release profile, the drug loaded scaffolds were immersed in individual centrifuge tubes containing 0.5 mL of phosphate buffer saline (PBS, pH 7.4) solution, and all of the tubes were kept in a shaking water bath at 37 °C. The PBS solutions were replaced with fresh PBS solutions at predetermined time intervals, and the collected supernatants at each time point were stored at −80 °C before analysis. The RVS and SrRn concentrations in the releasates were measured using a UV spectrophotometer at the wavelengths of 305 and 318 nm, respectively [35, 36]. The drug-release studies were performed by using five samples for each of the conditions.

2.3 Mouse mesenchymal stem cell (mMSC) culture, seeding, and differentiation

The mMSCs were previously isolated from bone marrow flushes of female FVB mice, as previously described [37]. They were provided by Dr. Leah Cook and are well characterized [38]. The mMSCs were cultured in growth medium consisting of low-glucose DMEM (GE Healthcare Life Sciences), 10% (v/v) fetal bovine serum (FBS, Sigma-Aldrich), 1% penicillin-streptomycin (P/S, Gibco), and platelet-derived growth factor AA (1 μg/100 ml, PeproTech) in 5% CO_2 at 37 °C. The cells were harvested using TrypLE (Gibco), resuspended in growth medium, and seeded onto each scaffold (1×10^5 cells in 50 μL of growth medium). After 4 h incubation for cell attachment, the growth medium was added. Differentiation was induced 3 days after seeding by replacing the growth medium with the differentiation medium consisting of growth medium plus 100 nM dexamethasone (Sigma), 10 mM β-glycerophosphate (Sigma), and 50 μM ascorbic acid (Sigma) and cultured for another 14 days [39]. Medium was replaced every second day.

The viability of mMSCs seeded on different scaffolds was evaluated by using a Live/Dead assay after 14-day culture [40, 41]. A confocal laser scanning microscope (CLSM, LSM 710, Carl Zeiss) was used to obtain fluorescent images. The cell proliferation of mMSCs on the scaffolds was examined at days 3, 7, and 14 by using an MTT assay [42, 43].

Alkaline Phosphatase (ALP) staining was conducted after 14-day differentiation by using an ALP leukocyte kit (Sigma Aldrich), according to the manufacturer's instructions [44]. The ALP activity was measured based on our previous method [45].

2.4 Osteoclast induction, culture, and characterization

Osteoclasts were differentiated from primary human peripheral blood monocytes, which were provided by the Elutriation Core Facility at the University of Nebraska Medical Center. The monocytes were seeded at a density of 1×10^5 cells/well in 24 well plates and differentiated using osteoclast induction medium, consisting of RPMI medium (Gibco), 10% FBS, 1% P/S, 25 ng/ml macrophage colony-stimulating factor (M-CSF, Stemcell), and 50 ng/ml receptor activator of nuclear factor-κB ligand (RANKL, Peprotech) for 14 days.

In order to test the response of osteoclasts to the released drugs, the scaffolds (⌀=6 mm), with or without drugs, were conditioned in the osteoclast differentiation medium at 37 °C for 3 days, and the media were collected (Fig. 1B). Then the differentiated osteoclasts were cultured in the medium (1 ml) containing released drugs for another 2 days. A tartrate-resistant acid phosphatase (TRAP) staining kit (Sigma) was used to evaluate the differentiation of TRAP-positive osteoclasts. The purple colored stained osteoclasts were randomly imaged using an inverted microscope, and the sizes of positive cells were measured and calculated using ImageJ software (at least three images were taken from each sample, and 5 samples were used for each scaffold group). TRAP activity was also measured by the conversion of p-nitrophenyl phosphate (pNPP) to p-nitrophenol (pNP) in the presence of sodium tartrate [46]. The osteoclasts were lysed with lysis buffer and subjected to a freeze-thaw cycle. A cell lysate sample was added to pNPP solution, incubated for 1 h at 37 °C, and then converted to pNP by adding 0.3 M NaOH. The absorbance at the wavelength of 405 nm was detected using a microplate reader. The total protein content was quantified by a Micro BCA Protein assay kit (Pierce). TRAP activity was expressed as μmol of pNP generated per minute per milligram of total proteins (μmol/min/mg protein).

2.5 Human umbilical vein endothelial cell (HUVEC) culture and characterization

HUVECs (Lonza) were grown in endothelial cell basal medium-2 (EGM-2 BulletKit, Lonza) used until passage 6. The cells were cultured in 5% CO_2 at 37 °C, and the medium was replaced every two days. The scaffolds were incubated in the EGM-2 medium at 37 °C for 3 days (Fig. 1B) and then collected. Tube formation and wound healing assays were conducted to evaluate the *in vitro* angiogenesis and migration. For the tube formation assay, each well of a 96-well plate was filled with 50 μl of cold matrigel and then incubated at 37 °C for 1 h. After the gel formation, HUVECs (1×10^5 cells/ml, 100 μl/well) were seeded in the matrigel-coated wells and cultured in the medium containing the released drugs from the different scaffolds for 16 h. The formed tubes were observed and photographed randomly with an inverted microscope (Leica). The tube nodes formed by HUVECs in each image were calculated using ImageJ software (at least three images were taken from each sample, and 5 samples were used for each scaffold group). For the migration assay, the 24-well plate was first coated with 300 μl of diluted matrigel (1:100) at 37 °C for 3 h. Then HUVECs were seeded in the coated plates. When the HUVECs reached 70% confluency, a 200 μl sterile pipette tip was used to make a scratch on the cell layer. The un-detached HUVECs were washed three times with PBS buffer and then cultured in medium containing released drugs from different scaffolds. Images of the scratch and the migaration of HUVECs from one edge of the scratch to the other side were taken immediately (t_0 = 0 h) and after 16 h of culture (t_{16} = 16 h) under an inverted microscope. The migration rate was calculated according to the formula: wound closure%= [(wound length at t_0 - wound length at t_{16}) / wound length at t_0] × 100 %. At least three images were randomly taken from each sample, and 4 samples were used for each scaffold group.

2.6 RNA isolation and quantitative real time polymerase chain reaction (PCR)

Total RNA was extracted from the cell-laden scaffolds or cell monolayers using QIA-Shredder and RNeasy mini-kits (QIAgen). Total RNA was transcribed into complementary DNA (cDNA) using an iScript cDNA synthesis kit (BioRad Laboratories). Real-time PCR

analysis was performed in a StepOnePlus™ Real-Time PCR System (Thermo Scientific) using SYBR Green Supermix (Bio-Rad). The cDNA samples were analyzed for the genes of interest and for the housekeeping gene 18S rRNA. The relative expression of each target gene was calculated using the comparative Ct ($2^{-\Delta\Delta Ct}$) method [47].

2.7 Critical-size rat mandibular defect model

The animal experiment was approved by the University of Nebraska Medical Center (UNMC) Animal Care and Use Committee. Sprague Dawley rats (male, weight 280 – 330 g) purchased from Charles River were used. They were anesthetized with an intramuscular administration of ketamine and xylazine. The surgical areas were shaved, and the skin was sterilized before surgical incision. A longitudinal incision was made along the left mandibular angle. The branches of facial nerves were protected from injuries. The masseter muscle was detached from the mandibular angle, and the outside of the mandibular bone was visible. A full-thickness 4-mm circular defect was drilled through in the mandibular angle with a trephine bur. The 3D printed scaffold was placed into the defect. The muscle and skin incision were closed. Five rats were included in the bone defect only group, six rats in the scaffolds only group, and another six rats in the scaffolds containing both RVS and SrRn group. Routine inspection was carried out in accordance with the protocol. At week 8 after surgery and implantation, the rats were euthanized. The left mandibular bone was collected, and bone formation was evaluated using micro computed tomography (CT) and histological staining.

2.9 Micro CT evaluation

The mandibular bones were fixed with paraformaldehyde and scanned with a high-resolution X-ray micro-CT scanner (SkyScan 1172) using a tube voltage of 55 kV, current of 181 μA, and a slice thickness/slice increment of 8.89 μm. The analysis of the micro-CT data was performed using CT analyzer software (Brucker micro-CT) [48]. From the multiple scan slices, a 3D reconstruction was performed using Micro-CT 3D visualization software. For evaluating new bone formation, the areas of the defect and 3D printed scaffold were selected as the region of interest (ROI). Bone volume (BV) and total volume (TV) in the ROI were measured, and the percentage of bone regeneration was calculated by dividing the bone volume to the total volume (BV/TV).

2.10 Histological staining

After micro-CT scanning, the bone samples were decalcified, paraffin embedded, sectioned into 6-μm slices, and subjected to hematoxylin-eosin (H&E) and Masson's Trichrome staining [49]. Histological staining images were acquired with an optical microscope.

2.11 Statistical analysis

All quantitative data are expressed as the mean ± standard deviation (SD). Statistical analysis was performed using ANOVA with Scheffé post-hoc tests. A p-value of < 0.05 was considered statistically significant.

3. Results

3.1 3D printing of small molecule loaded scaffolds and their characterization

We integrated a hydrogel-based bioink together with composite PCL/TCP to generate 3D bone constructs. RVS is hydrophobic and can be easily dissolved in the organic solvent with PCL/TCP. SrRn is freely soluble in acidic aqueous solutions, but it is slightly soluble in pure water (~3.7 mg/ml) [50]. In this study, we used a relatively low concentration (1 mg/ml) of SrRn in the Me-HA/Me-Gel based bioink. These two inks, with or without small molecule drugs, were printed in an alternating order (Fig. 1A). PCL/TCP was printed first, followed by 3D printing of the hydrogel in the groove created by the first material on the same layer. Then, layer-by-layer, we printed the initial large constructs with a square shape. The thickness is comparable to the mandibular bone thickness in the rat model. The punched scaffolds with various drugs were shown in Fig. 2A. The scaffolds were porous, and the scaffolds with RVS showed slightly yellowish color. To confirm the morphology, the 3D printed scaffolds, with or without drugs, were observed by SEM. Fig. 2B shows that all of the scaffolds had the PCL/TCP strut size of approximately 400 μm and that the hydrogels were successfully printed next to PCL/TCP, with a width of approximately 400 μm. The incorporation of small molecules did not affect the printing process or the printed scaffold structure.

The 3D printed scaffolds loaded with RVS and SrRn were subjected to *in vitro* release studies for 3 weeks. The small molecule loading amount was calculated to be 1.01 ± 0.05 μg/mg scaffold for RVS and 0.58 ± 0.02 μg/mg scaffold for SrRn. Since RVS loaded PCL/TCP were printed as the frame structure and SrRn loaded hydrogels were printed in between, more PCL/TCP, and thus RVS, were in the printed scaffolds. The cumulative release profiles of RVS and SrRn from the 3D printed scaffolds were shown in Fig. 2C. *In vitro* release studies demonstrated that SrRn had a significant burst release, resulting in more than 70% of the total drug being released at day 1. After the burst release stage, SrRn had sustained release for at least 21 days. In contrast, the release of RVS was very slow, and less than 30% of RVS was released throughout the 21-day release period. It is well known that PCL has a very slow degradation rate. Although TCP has a faster degradation rate compared to hydroxyapatite, the overall degradation rate of the composite scaffold is also slow. After the 21-day release study, all scaffolds were observed to not shrink, curl, or delaminate.

3.2 Effects of scaffolds on proliferation and osteogenic differentiation of mMSCs

We first seeded mMSCs onto various scaffolds to evaluate cell viability and the effects of drug release on mMSC osteogenic differentiation. The cells cultured on all of the scaffolds, with or without small molecules, showed high cell viability, and very few dead cells were observed (Fig. 3A). All the cells were well attached and showed a normal spreading morphology. An MTT assay was performed to determine the proliferation of mMSCs on the scaffolds. The results showed that the cells proliferated well on all of the scaffold groups with the increase of the culture time (Fig. 3B). The proliferation rate on the scaffolds with SrRn was highest throughout 14-day culture and was significantly higher than that on the scaffold alone and scaffolds with RVS at day 7. However, the MTT absorbance for mMSCs on all of the scaffold groups were comparable after 14-day culture.

After standard osteogenic induction, mMSCs on all of the scaffolds were positive to ALP staining (Fig. 3C). The 3D printed scaffolds loaded with both RVS and SrRn showed significantly higher ALP activity compared to the other three scaffold groups (Fig. 3D). Consistently, the ALP gene expression for mMSCs on RVS and SrRn loaded scaffolds was also significantly upregulated, as shown in Fig. 3E. The qPCR results also showed that the incorporation of SrRn within the scaffold statistically increased the expression of Runt-related transcription factor 2 (RUNX 2), osteocalcin (OCN), and collagen 1A1 (Col 1A1) (Fig. 3E). These results demonstrated that the combination of RVS and SrRn within the 3D printed scaffolds significantly promoted mMSC osteogenic differentiation.

3.3 Effects of released small molecules on monocyte induced osteoclast behaviors

In order to determine the effects of 3D printed scaffolds, with or without small molecules, on osteoclast activities, we incubated the scaffolds in osteoclast induction medium for 3 days and then utilized the released medium to treat human primary monocyte induced osteoclasts for another 2 days. As shown in Fig. S1, osteoclast-like cells with multiple nuclei and positive expression of F-actin ring and cathepsin-K were successfully differentiated from monocytes after 14-day induction. After 3-day incubation, the released RVS and SrRn were calculated to be 2.15 ± 0.13 μg/ml and 7.59 ± 0.40 μg/ml, respectively. We first evaluated the effects of the released small molecules on osteoclast morphology and size. Fig. 4A shows that the osteoclasts were positive to TRAP staining, and the size and number of the osteoclasts were decreased after incubation in the medium containing released small molecules. The quantitative measurement of osteoclast sizes confirmed that all of the treatments with released RVS, SrRn, or their combination significantly decreased osteoclast size, compared to the scaffold alone group (Fig. 4B). The osteoclasts had the smallest size after culture in the media with released SrRn. The TRAP activity was also evaluated, as shown in Fig. 4C. No significant difference was found between the scaffold alone and scaffold with RVS groups. However, compared to these groups, the other two groups with released SrRn showed significantly decreased TRAP activity.

We further examined gene expression of nuclear factor of activated T cells 1 (NFATc1), matrix metalloproteinase-9 (MMP-9), and cathepsin K (CTSK). NFATc1 is an important transcription factor that is required for sufficient osteoclast differentiation [51]. MMP-9 is a type IV collagenase and is highly expressed in osteoclasts [52]. MMP-9 plays an important role in extracellular matrix degradation and cell migration. Both NFATc1 and MMP-9 are upregulated at the early stage of osteoclastogenesis [53]. CTSK is predominantly expressed by multinucleated osteoclasts and can degrade collagen and other matrix proteins during bone resorption. The qPCR results showed that the released SrRn significantly downregulated the expression of NFATc1 and MMP-9, but it did not change the expression of CTSK (Fig. 4D). In contrast, RVS increased the expression of NFATc1 and had no effects on MMP-9 and CTSK expression. The combination release of SrRn and RVS only downregulated NFATc1expression but not MMP-9.

3.4 Effects of released small molecules on HUVEC tube formation and migration

Released medium (EGM medium) with RVS, SrRn, or their combination was also collected to condition HUVECs. A tube formation assay was conducted to evaluate *in vitro*

angiogenesis of HUVECs in response to various released small molecules. In this assay, HUVECs were seeded onto the Matrigel (containing basement membrane matrix) and developed a vascular tubular structure (Fig. S2A). The numbers of branch sites/nodes were quantified. As shown in Fig. 5A, the node density for HUVECs was significantly increased after incubation in all the three types of release media, compared to the scaffold alone group. No statistical difference was seen among the three groups with various small molecules. We also determined how the release medium affected HUVEC migration by using a wound healing assay. The “wound” was created on the confluent monolayer of HUVECs by the mechanical removal of a portion of cells using a pipette tip. Then the HUVECs started migrating to heal the “wound” (Fig. S2B). After 16 h migration, we found that HUVECs treated with RVS medium showed the highest wound closure ratio, which was significantly higher than in scaffold alone and SrRn groups (Fig. 5B).

We also examined the gene expression of vascular endothelial growth factor A (VEGFA), platelet-endothelial cell adhesion molecule (PECAM)-1, and von Willebrand factor (vWF), all of which are important for angiogenesis and HUVEC functions. The qPCR results demonstrated that HUVECs had the highest levels of VEGFA, PECAM, and vWF gene expression in the RVS release medium, compared to those in other release medium conditions (Fig. 5C). Moreover, the medium with both RVS and SrRn also significantly upregulated angiogenesis related gene expression, compared to scaffold alone and SrRn groups.

3.5 3D printed scaffolds with dual small molecules promoted *in vivo* bone formation

To evaluate bone regeneration, we implanted the 3D printed scaffolds into rats with critical-size mandibular bone defects for 8 weeks (Fig. 6A). Since the incorporation of both RVS and SrRn showed promising combinational effects on osteogenesis, angiogenesis, and osteoclast inhibition *in vitro*, we implemented the scaffolds with both small molecules and the scaffold alone as the control for the mandibular implantation and compared their *in vivo* bone formation capacity. The harvested mandibular bone samples were first scanned using micro-CT, to evaluate the bone healing. Representative 3D reconstructions of the micro-CT images for the various implant groups are shown in Fig. 6B. After 8-week implantation, the defect only group showed unfilled defects with very limited bone regeneration. In the scaffold only group, some new bone formation at the periphery of the bone defects was observed, but the center of the defect was still filled with scaffold rather than bone tissue. The 3D printed scaffolds with the incorporation of RVS and SrRn facilitated bone formation (Fig. 6B). The formed new bones were detected not only around the scaffold struts but also on the top of the scaffold. A quantitative measurement of new bone volume percentage (BV/TV ratio), based on micro-CT analysis, confirmed that the 3D printed scaffolds with both RVS and SrRn elicited remarkable new bone formation in comparison to the other two groups (Fig. 6C) After 8-week implantation, all of the composite scaffolds were still detectable, as expected.

Histological and immunofluorescent stainings were performed after micro-CT analysis to confirm the extent of bone formation and vascularization. For H&E staining, connective soft tissues, rather than mineralized tissues, were observed in the defect only group without any

scaffold implantation (Fig. 7A). In contrast, new bone tissue formation partially occurred in the defect implanted with 3D printed scaffolds. Notably, new bone formation in the defect implanted with RVS and SrRn loaded 3D printed scaffolds occurred at the periphery as well as the center of the defect. In Masson's Trichrome staining (Fig. 7B), blue represents mineralized collagen tissue and red indicates muscle fibers. The staining results also confirmed that more new bone formation was observed in defect sites treated with dual small molecule loaded 3D printed scaffolds.

4. Discussion

It is well known that bone is a metabolic organ that possesses properties of osteoclastic bone resorption and osteogenic bone formation [54]. The bone marrow derived MSCs, osteoblasts, and osteoclasts play important roles in modulating mineral homeostasis [55]. Vascularization can have a great effect on bone regeneration by increasing the delivery of nutrients, oxygen, growth factors, and stem cells[56]. Our current study aims to fabricate 3D printed scaffolds with the incorporation of multiple small molecules to target multiple bone cell types (i.e. MSCs, osteoclasts, and endothelial cells) for promoting bone regeneration.

We implemented RVS and SrRn to demonstrate the feasibility and *in vivo* efficacy. RVS is soluble in organic solvents, while SrRn is water soluble. These two small molecule drugs were thus incorporated into a PCL/TCP-based ink and a Me-HA/Me-Gel-based bioink, respectively. Ideally, the incorporated small molecules should be released in a stable and sustainable manner in order to provide continuous bioactivities on targets [57]. In our study, RVS had a very limited burst release, while SrRn showed a significant burst release in first 24 hours in PBS solution. Both RVS and SrRn had sustained release over 3 weeks. A study from Tian et al. also showed a similar release profile of SrRn from a chitosan film coated onto a titanium surface [58]. We have used a similar strategy to fabricate 3D printed scaffolds loaded with multiple antibiotics to mitigate an established biofilm and clear craniotomy-associated infection [32].

RVS was reported to increase ALP activity via SIRT1 activation of BMP2 [59, 60], induce osteoblastic differentiation [61], and promote mineralization of mMSCs [62]. RVS also activated the Wnt/β-catenin signaling pathway, upregulated lncRNA KCNQ1OT1, and inhibited polymethylmethacrylate particle-induced osteolysis in a mouse model [63]. In late stages of osteogenic differentiation, RVS activated Notch signaling to promote differentiation of osteoblasts into osteocytes [64]. Previous studies showed that RVS could also inhibit the osteoclastogenesis to reduce alveolar bone loss [65] and improved angiogenesis [66] in rodent models. Our results are consistent with reported studies and demonstrate that the 3D printed scaffolds with RVS promoted osteogenic differentiation of MSCs. The pharmacological effects of RVS on cell proliferation are closely related to drug dose/concentration [67, 68]. RVS was found to enhance the proliferation of human umbilical cord derived MSCs (hUC-MSCs) at concentrations from 0.1 μM to 2.5 μM. However, increased doses of RVS (from 5 μM to 10 μM) conversely decreased the growth of hUC-MSCs [69]. A higher concentration of RVS (25 μM) was reported to have a negative impact on MSCs proliferation but promote osteogenic differentiation [70]. In our study, the controlled release of RVS did not significantly affect mMSC proliferation, demonstrating its

safety. The effects of RVS on endothelial cells are also dose dependent [71]. At a low concentration, RVS was reported to increase HUVEC migration and tube formation, whereas a high concentration of RVS inhibited HUVEC angiogenesis [72]. Our results demonstrated that the concentration of sustained-release RVS was in a safe and effective range to promote HUVEC angiogenesis *in vitro*.

Also, in our study, SrRn was incorporated to target MSCs/osteoblasts and osteoclasts. SrRn was previously reported to possess properties that affect bone metabolism, including inhibition of osteoclastic resorption and promotion of osteogenesis [73–76]. SrRn has been approved in Europe since 2004 for the treatment of osteoporosis [77]. SrRn has been demonstrated to enhance trabecular thickness and bone volume in both pre-clinical models and human studies [77, 78]. The fundamental mechanisms have been extensively investigated. It was reported that the osteogenic improvement by Sr ions involved the overexpression of the ROCK1 [79] and Setd2 genes [80], Wnt/β-catenin pathway activation [81], and NF-kB signaling inhibition [82]. SrRn also enhanced angiogenesis [83] via activating the PI3K/AKT/mTOR signaling pathway [84] and regulating the inflammatory response during *in vivo* bone formation [85]. Similar to RVS, the effects of SrRn also are also dose dependent [85, 86]. For example, 5% SrRn mixed with PCL/polydiisopropyl fumarate (PDIPF) was more likely to increase inflammation and inhibit osteogenesis, while PCL/PDIPF with 1% SrRn could stimulate new bone formation [87]. In our study, we demonstrated that SrRn promoted osteogenic differentiation of mMSCs and HUVEC migration and tube formation. Most importantly, SrRn significantly decreased osteoclast size, activity, and gene expression.

As previously discussed, many studies noted that both RVS and SrRn had effects on various bone related cells, but very few studies have evaluated their comparative pharmacological activities and evaluated their potential synergistic effects on bone regeneration. In our current study, the 3D printed scaffolds with the incorporation of both RVS and SrRn combined the features of RVS and SrRn for promoting angiogenesis and inhibiting osteoclast activities at the same time. The released RVS and SrRn also showed synergistic effects on osteogenic differentiation of MSC. We further implemented a rat model with a critical-size mandibular bone defect and implanted the 3D printed scaffolds with and without the dual small molecules. Our 3D printed scaffolds with combined release of RVS and SrRn significantly improved bone formation. There are multiple factors contributing to the enhanced bone regeneration in our study. The sustained release of low dose RVS may promote angiogenesis and enhance bone formation by facilitating osteogenesis of progenitor cells and stem cells. The released SrRn may temporally inhibit osteoclastogenesis and thus may decrease bone resorption. The effects of RVS and SrRn may be synergistic or additive, and many signaling pathways may potentially be involved.

In order to enhance the regeneration efficacy of bone tissue engineering scaffolds, growth factors have been incorporated into the scaffolds, often resulting in improved outcomes [88]. However, despite reported success in animals, the clinical use of growth factor-impregnated scaffolds is still hampered by a number of challenges, including stability, cost, and control of the release rate [89]. Many small molecules have been identified to possess bioactivity similar to growth factors and could mimic their function *in vivo* [90]. The application of

small molecules within scaffolds is becoming a potential alternative to growth factors, as they can overcome many disadvantages related to growth factors, particularly with stability, convenience, and immunogenicity. Addressing the interdependence of angiogenesis and osteogenesis, multiple growth factors have been loaded into scaffolds to simultaneously promote angiogenesis and osteogenesis in order to improve bone regeneration [91, 92]. However, this strategy is highly complicated, and the dose and delivery of different growth factors need to be tailored carefully to reduce the potential for untoward side effects. Our studies show that the combined use of the small molecules such as RVS and SrRn loaded into bioprinted scaffolds can improve bone formation *in vivo* and is a promising alternative to multi-growth factor approaches previously reported.

One limitation of the current study is that SrRn is not released in a well-controlled manner due to its water solubility. Although SrRn can affect osteoclastogenesis at a relatively low concentration, the medium extracted after 3-day release may not have any effect on osteoclasts and HUVECs. For the *in vivo* implantation, the composite scaffolds may have a slower release rate in the bone environment compared to under aqueous *in vitro* conditions. A more stable and sustained release pattern might improve the pharmacological effects. In order to reduce or altogether eliminate the burst release of loaded SrRn, a valid and stable delivery system should be established. For example, we can fabricate microspheres loaded with SrRn in the future and incorporate the SrRn loaded microspheres into the hydrogel-based bioink for the scaffold fabrication.

5. Conclusion

In summary, we implemented multiple bioinks to 3D print bone scaffolds loaded with two small bioactive molecules, RVS and SrRn. RVS had a more sustained release profile, while SrRn had an initial burst release then a sustained release for three weeks. The release of RVS and SrRn from the 3D printed scaffolds targeted multiple cells, including MSCs, endothelial cells, and osteoclasts. The released RVS significantly promoted HUVEC migration, tube-like structure formation, and angiogenic gene expression *in vitro*. The 3D printed scaffolds with SrRn also greatly increased mMSC proliferation and osteogenic differentiation. Both RVS and SrRn decreased osteoclast size, and the released SrRn also significantly decreased osteoclast activities and related gene expression. The bone scaffolds with both RVS and SrRn had combinational advantages in enhancing angiogenesis, inhibiting osteoclast activities, and synergistically promoting mMSC osteogenic differentiation. We further demonstrated that the 3D printed scaffolds with small molecules significantly promoted bone formation after implantation in rats with critical-sized mandibular bone defects.

Supplementary Material

Refer to Web version on PubMed Central for supplementary material.

Acknowledgements

This work has been supported by Mary & Dick Holland Regenerative Medicine Program start-up grant and pilot grant, Nebraska Research Initiative Funding, University of Nebraska Collaboration Initiative Seed Grant, NIH (R01 AR073225) to Dr. Bin Duan. NIH (R21AI140026) to Drs. Patrick Reid and Bin Duan. Xiping Jiang is partially supported by the China Scholarship Council. Support for the UNMC Advanced Microscopy Core Facility was

provided by the Nebraska Research Initiative, the Fred and Pamela Buffett Cancer Center Support Grant (P30CA036727), and an Institutional Development Award (IDeA) from the NIGMS of the NIH (P30GM106397). The authors declare no competing financial interest. The Electron Microscopy Core Facility (EMCF) at UNMC is supported by state funds from the Nebraska Research Initiative and the University of Nebraska Foundation, and institutionally by the Office of the Vice Chancellor for Research.

References

[1]. Salyer KE, Taylor DP, Bone grafts in craniofacial surgery, Clinics in Plastic Surgery 14 (1987) 27–35. [PubMed: 3545620]

[2]. Gaihre B, Uswatta S, Jayasuriya AC, Reconstruction of craniomaxillofacial bone defects using tissue-engineering strategies with injectable and non-injectable scaffolds., Journal of Functional Biomaterials 8 (2017) E49. [PubMed: 29156629]

[3]. Zaky SH, Cancedda R, Engineering craniofacial structures: Facing the challenge, Journal of Dental Research 88 (2009) 1077–1091. [PubMed: 19897785]

[4]. Ghassemi T, Shahroodi A, Ebrahimzadeh MH, Mousavian A, Movaffagh J, Moradi A, Current concepts in scaffolding for bone tissue engineering, Archives of Bone and Joint Surgery 6 (2018) 90–99. [PubMed: 29600260]

[5]. Borrelli MR, Hu MS, Longaker MT, Lorenz HP, Tissue engineering and regenerative medicine in craniofacial reconstruction and facial aesthetics, Journal of Craniofacial Surgery (2019) doi: 10.1097/SCS.0000000000005840.

[6]. Roasa FV, Castañeda SS, Mendoza DJC, Pediatric free flap reconstruction for head and neck defects, Current opinion in otolaryngology & head and neck surgery 26 (2018) 334–339. [PubMed: 30074517]

[7]. Zhang W, Yelick PC, Craniofacial tissue engineering, Cold Spring Harbor Perspectives in Medicine 8 (2018) a025775. [PubMed: 28348178]

[8]. Amini AR, Laurencin CT, Nukavarapu SP, Bone tissue engineering: Recent advances and challenges, Critical Reviews in Biomedical Engineering 40 (2012) 363–408. [PubMed: 23339648]

[9]. Bose S, Vahabzadeh S, Bandyopadhyay A, Bone tissue engineering using 3D printing, Materials Today 16 (2013) 496–504.

[10]. Mok SW, Nizak R, Fu SC, Ho KWK, Qin L, Saris DBF, Chan KM, Malda J, From the printer: Potential of three-dimensional printing for orthopaedic applications, Journal of Orthopaedic Translation 6 (2016) 42–49. [PubMed: 30035082]

[11]. Nyberg EL, Farris AL, Hung BP, Dias M, Garcia JR, Dorafshar AH, Grayson WL, 3D-printing technologies for craniofacial rehabilitation, reconstruction, and regeneration, Annals of Biomedical Engineering 45 (2017) 45–57. [PubMed: 27295184]

[12]. Maroulakos M, Kamperos G, Tayebi L, Halazonetis D, Ren Y, Applications of 3D printing on craniofacial bone repair: A systematic review, Journal of Dentistry 80 (2019) 1–14. [PubMed: 30439546]

[13]. Wang MO, Vorwald CE, Dreher ML, Mott EJ, Cheng MH, Cinar A, Mehdizadeh H, Somo S, Dean D, Brey EM, Fisher JP, Evaluating 3D-printed biomaterials as scaffolds for vascularized bone tissue engineering, Advanced Materials 27 (2014) 138–144. [PubMed: 25387454]

[14]. Feng C, Zhang W, Deng C, Li G, Chang J, Zhang Z, Jiang X, Wu C, 3D printing of lotus root-like biomimetic materials for cell delivery and tissue regeneration, Advanced Science 4 (2017) 1700401. [PubMed: 29270348]

[15]. Pati F, Song TH, Rijal G, Jang J, Kim SW, Cho DW, Ornamenting 3D printed scaffolds with cell-laid extracellular matrix for bone tissue regeneration, Biomaterials 37 (2015) 230–241. [PubMed: 25453953]

[16]. Park JY, Shim JH, Choi SA, Jang J, Kim M, Lee SH, Cho DW, 3D printing technology to control BMP-2 and VEGF delivery spatially and temporally to promote large-volume bone regeneration, Journal of Materials Chemistry B 3 (2015) 5415–5425. [PubMed: 32262513]

[17]. Arvidson K, Abdallah BM, Applegate LA, Baldini N, Cenni E, Gomez-Barrena E, Granchi D, Kassem M, Konttinen YT, Mustafa K, Pioletti DP, Sillat T, Finne-Wistrand A, Bone regeneration and stem cells, Journal of Cellular Molecular Medicine 15 (2011) 718–746. [PubMed: 21129153]

[18]. Barati D, Shariati SRP, Moeinzadeh S, Melero-Martin JM, Khademhosseini A, Spatiotemporal release of BMP-2 and VEGF enhances osteogenic and vasculogenic differentiation of human mesenchymal stem cells and endothelial colony-forming cells co-encapsulated in a patterned hydrogel, Journal of Controlled Release 223 (2016) 126–136. [PubMed: 26721447]

[19]. Cui H, Zhu W, Nowicki M, Zhou X, Khademhosseini A, Zhang LG, Hierarchical fabrication of engineered vascularized bone biphasic constructs via dual 3D bioprinting: Integrating regional bioactive factors into architectural design, Advanced Healthcare Materials 5 (2016) 2174–2181. [PubMed: 27383032]

[20]. Ashammakhi N, Ahadian S, Xu C, Montazerian H, Ko H, Nasiri R, Barros N, Khademhosseini A, Bioinks and bioprinting technologies to make heterogeneous and biomimetic tissue constructs, Materials Today Bio 1 (2019) 100008.

[21]. Aravamudhan A, Ramos DM, Nip J, Subramanian A, James R, Harmon MD, Yu X, Kumbar SG, Osteoinductive small molecules: Growth factor alternatives for bone tissue engineering, Current Pharmaceutical Design 19 (2013) 3420–3428. [PubMed: 23432678]

[22]. Goonoo N, Bhaw-Luximon A, Mimicking growth factors: Role of small molecule scaffold additives in promoting tissue regeneration and repair, RSC Advances 9 (2019) 18124–18146.

[23]. Bhat KPL, Kosmeder II JW, Pezzuto JM, Biological effects of resveratrol, Antioxidants and Redox Signaling 3 (2001) 1041–1064. [PubMed: 11813979]

[24]. Zhu X, Liu Q, Wang M, Liang M, Yang X, Xu X, Zou H, Qiu J, Activation of Sirt1 by resveratrol inhibits TNF-α induced inflammation in fibroblasts, PLoS ONE 6 (2011) e27081. [PubMed: 22069489]

[25]. Gülçin I, Antioxidant properties of resveratrol: A structure-activity insight, Innovative Food Science and Emerging Technologies 11 (2010) 210–218.

[26]. Fulda S, Debatin KM, Sensitization for anticancer drug-induced apoptosis by the chemopreventive agent resveratrol, Oncogene 23 (2004) 6702–6711. [PubMed: 15273734]

[27]. Yan F, Sun X, Xu C, Protective effects of resveratrol improve cardiovascular function in rats with diabetes, Experimental and Therapeutic Medicine 15 (2018) 1728–1734. [PubMed: 29434758]

[28]. Li Y, Dnmark S, Edlund U, Finne-Wistrand A, He X, Norgrd M, Blomén E, Hultenby K, Andersson G, Lindgren U, Resveratrol-conjugated poly - Caprolactone facilitates in vitro mineralization and in vivo bone regeneration, Acta Biomaterialia (2011) 751–758. [PubMed: 20849988]

[29]. Rutledge KE, Cheng Q, Jabbarzadeh E, Modulation of inflammatory response and induction of bone formation based on combinatorial effects of resveratrol, Journal of Nanomedicine and Nanotechnology 7 (2016) 350. [PubMed: 27175310]

[30]. Marie PJ, Strontium ranelate: A physiological approach for optimizing bone formation and resorption, Bone 38 (2006) 10–14.

[31]. Bonnelye E, Chabadel A, Saltel F, Jurdic P, Dual effect of strontium ranelate: Stimulation of osteoblast differentiation and inhibition of osteoclast formation and resorption in vitro, Bone 42 (2008) 129–138. [PubMed: 17945546]

[32]. Aldrich A, Kuss MA, Duan B, Kielian T, 3D bioprinted scaffolds containing viable macrophages and antibiotics promote clearance of staphylococcus aureus craniotomy-associated biofilm infection, ACS Applied Materials and Interfaces 11 (2019) 12298–12307. [PubMed: 30855125]

[33]. Kuss MA, Wu S, Wang Y, Untrauer JB, Li W, Lim JY, Duan B, Prevascularization of 3D printed bone scaffolds by bioactive hydrogels and cell co-culture, J Biomed Mater Res B Appl Biomater 106(5) (2018) 1788–1798. [PubMed: 28901689]

[34]. Wang Y, Wu S, Kuss M, Streubel P, Duan B, Effects of hydroxyapatite and hypoxia on chondrogenesis and hypertrophy in 3D bioprinted ADMSC laden constructs, ACS Biomaterials Science & Engineering 3 (2017) 826–835. [PubMed: 33440487]

[35]. Poornima B, Korrapati PS, Fabrication of chitosan-polycaprolactone composite nanofibrous scaffold for simultaneous delivery of ferulic acid and resveratrol, Carbohydrate Polymers 157 (2017) 1741–1749. [PubMed: 27987890]

[36]. Nair B, Sindhu M, Nair PD, Polycaprolactone-laponite composite scaffold releasing strontium ranelate for bone tissue engineering applications, Colloids and Surfaces B: Biointerfaces 143 (2016) 423–430. [PubMed: 27037779]

[37]. Huang S, Xu L, Sun Y, Wu T, Wang K, Li G, An improved protocol for isolation and culture of mesenchymal stem cells from mouse bone marrow, Journal of Orthopaedic Translation 3 (2015) 26–33. [PubMed: 30035037]

[38]. Cook LM, Frieling JS, Nerlakanti N, McGuire JJ, Stewart PA, Burger KL, Cleveland JL, Lynch CC, Betaglycan drives the mesenchymal stromal cell osteogenic program and prostate cancer-induced osteogenesis, Oncogene 38 (2019) 6959–6969. [PubMed: 31409900]

[39]. Kuss MA, Wu S, Wang Y, Untrauer JB, Li W, Lim JY, Duan B, Prevascularization of 3D printed bone scaffolds by bioactive hydrogels and cell co-culture, Journal of Biomedical Materials Research Part B: Applied Biomaterials 106(5) (2018) 1788–1798. [PubMed: 28901689]

[40]. Wu S, Duan B, Liu P, Zhang C, Qin X, Butcher JT, Fabrication of Aligned Nanofiber Polymer Yarn Networks for Anisotropic Soft Tissue Scaffolds, ACS applied materials & interfaces 8(26) (2016) 16950–16960. [PubMed: 27304080]

[41]. Shi W, Hass B, Kuss MA, Zhang H, Ryu S, Zhang D, Li T, Li YL, Duan B, Fabrication of versatile dynamic hyaluronic acid-based hydrogels, Carbohydr Polym 233 (2020) 115803. [PubMed: 32059877]

[42]. Wu S, Peng H, Li X, Streubel PN, Liu Y, Duan B, Effect of scaffold morphology and cell co-culture on tenogenic differentiation of HADMSC on centrifugal melt electrospun poly (L−lactic acid) fibrous meshes, Biofabrication 9(4) (2017) 044106. [PubMed: 29134948]

[43]. Wang Y, Shi W, Kuss MA, Mirza S, Qi D, Krasnoslobodtsev A, Zeng J, Band H, Band V, Duan B, 3D Bioprinting of Breast Cancer Models for Drug Resistance Study, ACS Biomaterials Science & Engineering (2018).

[44]. Wang Y, Wu S, Kuss MA, Streubel PN, Duan B, Effects of Hydroxyapatite and Hypoxia on Chondrogenesis and Hypertrophy in 3D Bioprinted ADMSC Laden Constructs, ACS Biomaterials Science & Engineering 3(5) (2017) 826–835. [PubMed: 33440487]

[45]. Kuss MA, Wu S, Wang Y, Untrauer JB, Li W, Lim JY, Duan B, Prevascularization of 3D printed bone scaffolds by bioactive hydrogels and cell co-culture, Journal of Biomedical Materials Research Part B-Applied Biomaterials 106(5) (2018) 1788–1798.

[46]. Davison NL, ten Harkel B, Schoenmaker T, Luo X, Yuan H, Everts V, Barrère-de Groot F, de Bruijn JD, Osteoclast resorption of beta-tricalcium phosphate controlled by surface architecture, Biomaterials 35 (2014) 7441–7451. [PubMed: 24927681]

[47]. Wang Y, Shi W, Kuss M, Mirza S, Qi D, Krasnoslobodtsev A, Zeng J, Band H, Band V, Duan B, 3D bioprinting of breast cancer models for drug resistance study, ACS Biomaterials Science and Engineering 4 (2018) 4401–4411. [PubMed: 33418833]

[48]. Boda SK, Almoshari Y, Wang H, Wang X, Reinhardt RA, Duan B, Wang D, Xie J, Mineralized nanofiber segments coupled with calcium-binding BMP-2 peptides for alveolar bone regeneration, Acta Biomaterialia 85 (2019) 282–293. [PubMed: 30605770]

[49]. Kuss MA, Wu S, Wang Y, Untrauer JB, Li W, Lim JY, Duan B, Prevascularization of 3D printed bone scaffolds by bioactive hydrogels and cell co-culture, Journal of Biomedical Materials Research Part B: Applied Biomaterials (2017) DOI: 10.1002/jbm.b.33994.

[50]. Çelik A, Yalin S, Sağir O, Çömelekoğlu U, Eke D, Strontium ranelate induces genotoxicity in bone marrow and peripheral blood upon acute and chronic treatment, Journal of Cell and Molecular Biology 9 (2011) 27–35.

[51]. Crotti TN, Flannery M, Walsh NC, Fleming JD, Goldring SR, McHugh KP, NFATc1 regulation of the human β3 integrin promoter in osteoclast differentiation, Gene 372 (2006) 92–102. [PubMed: 16513293]

[52]. Sundaram K, Nishimura R, Senn J, Youssef RF, London SD, Reddy SV, RANK ligand signaling modulates the matrix metalloproteinase-9 gene expression during osteoclast differentiation, Experimental Cell Research 313 (2007) 168–178. [PubMed: 17084841]

[53]. Blair HC, Athanasou N, Recent advances in osteoclast biology and pathological bone resorption, Histology and Histopathology 19 (2004) 189–199. [PubMed: 14702187]

[54]. Burg KJ, Porter S, Kellam JF, Biomaterial developments for bone tissue engineering, Biomaterials 21(23) (2000) 2347–2359. [PubMed: 11055282]

[55]. Raggatt LJ, Partridge NC, Cellular and molecular mechanisms of bone remodeling, J Biol Chem 285(33) (2010) 25103–8. [PubMed: 20501658]

[56]. Xue Y, Xing Z, Hellem S, Arvidson K, Mustafa K, Endothelial cells influence the osteogenic potential of bone marrow stromal cells, BioMedical Engineering OnLine 8(1) (2009) 34. [PubMed: 19919705]

[57]. Li D, Chen K, Duan L, Fu T, Li J, Mu Z, Wang S, Zou Q, Chen L, Feng Y, Strontium Ranelate Incorporated Enzyme-Cross-Linked Gelatin Nanoparticle/Silk Fibroin Aerogel for Osteogenesis in OVX-Induced Osteoporosis, ACS Biomaterials Science & Engineering 5(3) (2019) 1440–1451. [PubMed: 33405619]

[58]. Tian A, Zhai J, Peng Y, Zhang L, Teng M, Liao J, Sun X, Liang X, Osteoblast response to titanium surfaces coated with strontium ranelate-loaded chitosan film, The International Journal of Oral & Maxillofacial Implants 29 (2014) 1446–1453. [PubMed: 25397808]

[59]. Choi Y, Yoon DS, Lee K-M, Choi SM, Lee M-H, Park KH, Han SH, Lee JW, Enhancement of Mesenchymal Stem Cell-Driven Bone Regeneration by Resveratrol-Mediated SOX2 Regulation, Aging and disease 10(4) (2019) 818. [PubMed: 31440387]

[60]. Zhao M, Ko SY, Garrett IR, Mundy GR, Gutierrez GE, Edwards JR, The polyphenol resveratrol promotes skeletal growth in mice through a sirtuin 1-bone morphogenic protein 2 longevity axis, British journal of pharmacology 175(21) (2018) 4183–4192. [PubMed: 30125963]

[61]. Bäckesjö CM, Li Y, Lindgren U, Haldosén LA, Activation of Sirt1 decreases adipocyte formation during osteoblast differentiation of mesenchymal stem cells, Journal of Bone and Mineral Research 21(7) (2006) 993–1002. [PubMed: 16813520]

[62]. Li Y, Dånmark S, Edlund U, Finne-Wistrand A, He X, Norgård M, Blomén E, Hultenby K, Andersson G, Lindgren U, Resveratrol-conjugated poly-ε-caprolactone facilitates in vitro mineralization and in vivo bone regeneration, Acta biomaterialia 7(2) (2011) 751–758. [PubMed: 20849988]

[63]. Gao X, Ge J, Li W, Zhou W, Xu L, LncRNA KCNQ1OT1 promotes osteogenic differentiation to relieve osteolysis via Wnt/β-catenin activation, Cell & bioscience 8(1) (2018) 19. [PubMed: 29541443]

[64]. Ji Y, Ke Y, Gao S, Intermittent activation of notch signaling promotes bone formation, American journal of translational research 9(6) (2017) 2933. [PubMed: 28670381]

[65]. Matsuda Y, Minagawa T, Okui T, Yamazaki K, Resveratrol suppresses the alveolar bone resorption induced by artificial trauma from occlusion in mice, Oral diseases 24(3) (2018) 412–421. [PubMed: 28944599]

[66]. Murgia D, Mauceri R, Campisi G, De Caro V, Advance on resveratrol application in bone regeneration: progress and perspectives for use in oral and maxillofacial surgery, Biomolecules 9(3) (2019) 94.

[67]. Safaeinejad Z, Kazeminasab F, Kiani-Esfahani A, Ghaedi K, Nasr-Esfahani MH, Multi-effects of resveratrol on stem cell characteristics: Effective dose, time, cell culture conditions and cell type-specific responses of stem cells to resveratrol, European journal of medicinal chemistry 155 (2018) 651–657. [PubMed: 29935438]

[68]. Hu C, Li L, The application of resveratrol to mesenchymal stromal cell-based regenerative medicine, Stem cell research & therapy 10(1) (2019) 307. [PubMed: 31623691]

[69]. Wang X, Ma S, Meng N, Yao N, Zhang K, Li Q, Zhang Y, Xing Q, Han K, Song J, Resveratrol exerts dosage-dependent effects on the self-renewal and neural differentiation of hUC-MSCs, Molecules and cells 39(5) (2016) 418. [PubMed: 27109421]

[70]. Ornstrup MJ, Harsløf T, Sørensen L, Stenkjær L, Langdahl BL, Pedersen SB, Resveratrol increases osteoblast differentiation in vitro independently of inflammation, Calcified tissue international 99(2) (2016) 155–163. [PubMed: 27000750]

[71]. LaFoya B, Munroe JA, Albig AR, A comparison of resveratrol and other polyphenolic compounds on Notch activation and endothelial cell activity, PloS one 14(1) (2019).

[72]. Wang Z, Wu Y, Wang J, Zhang C, Yan H, Zhu M, Wang K, Li C, Xu Q, Kong D, Effect of Resveratrol on Modulation of Endothelial Cells and Macrophages for Rapid Vascular Regeneration from Electrospun Poly (ε-caprolactone) Scaffolds, ACS applied materials & interfaces 9(23) (2017) 19541–19551. [PubMed: 28539044]

[73]. Quade M, Vater C, Schlootz S, Bolte J, Langanke R, Bretschneider H, Gelinsky M, Goodman SB, Zwingenberger S, Strontium enhances BMP-2 mediated bone regeneration in a femoral murine

bone defect model, Journal of Biomedical Materials Research Part B: Applied Biomaterials 108(1) (2020) 174–182. [PubMed: 30950569]

[74]. Jiménez M, Abradelo C, San Román J, Rojo L, Bibliographic review on the state of the art of strontium and zinc based regenerative therapies. Recent developments and clinical applications, Journal of materials chemistry B 7(12) (2019) 1974–1985. [PubMed: 32254801]

[75]. Autefage H, Allen F, Tang H, Kallepitis C, Gentleman E, Reznikov N, Nitiputri K, Nommeots-Nomm A, O'Donnell M, Lange C, Multiscale analyses reveal native-like lamellar bone repair and near perfect bone-contact with porous strontium-loaded bioactive glass, Biomaterials 209 (2019) 152–162. [PubMed: 31048149]

[76]. Bonnelye E, Chabadel A, Saltel F, Jurdic P, Dual effect of strontium ranelate: stimulation of osteoblast differentiation and inhibition of osteoclast formation and resorption in vitro, Bone 42(1) (2008) 129–138. [PubMed: 17945546]

[77]. Pilmane M, Salma-Ancane K, Loca D, Locs J, Berzina-Cimdina L, Strontium and strontium ranelate: Historical review of some of their functions, Materials Science and Engineering C 78 (2017) 1222–1230. [PubMed: 28575961]

[78]. Busse B, Jobke B, Hahn M, Priemel M, Niecke M, Seitz S, Zustin J, Semler J, Amling M, Effects of strontium ranelate administration on bisphosphonate-altered hydroxyapatite: Matrix incorporation of strontium is accompanied by changes in mineralization and microstructure, Acta biomaterialia 6(12) (2010) 4513–4521. [PubMed: 20654744]

[79]. Guo X, Wei S, Lu M, Shao Z, Lu J, Xia L, Lin K, Zou D, RNA-Seq investigation and in vivo study the effect of strontium ranelate on ovariectomized rat via the involvement of ROCK1, Artificial cells, nanomedicine, and biotechnology 46(sup1) (2018) 629–641.

[80]. Jia X, Long Q, Miron RJ, Yin C, Wei Y, Zhang Y, Wu M, Setd2 is associated with strontium-induced bone regeneration, Acta biomaterialia 53 (2017) 495–505. [PubMed: 28219807]

[81]. Yang F, Yang D, Tu J, Zheng Q, Cai L, Wang L, Strontium enhances osteogenic differentiation of mesenchymal stem cells and in vivo bone formation by activating Wnt/catenin signaling, Stem cells 29(6) (2011) 981–991. [PubMed: 21563277]

[82]. Yamaguchi M, Weitzmann MN, The intact strontium ranelate complex stimulates osteoblastogenesis and suppresses osteoclastogenesis by antagonizing NF-κB activation, Molecular and cellular biochemistry 359(1–2) (2012) 399–407. [PubMed: 21874315]

[83]. Prabha RD, Nair BP, Ditzel N, Kjems J, Nair PD, Kassem M, Strontium functionalized scaffold for bone tissue engineering, Materials Science and Engineering: C 94 (2019) 509–515. [PubMed: 30423735]

[84]. Guo X, Wei S, Lu M, Shao Z, Lu J, Xia L, Lin K, Zou D, Dose-dependent effects of strontium ranelate on ovariectomy rat bone marrow mesenchymal stem cells and human umbilical vein endothelial cells, International journal of biological sciences 12(12) (2016) 1511. [PubMed: 27994515]

[85]. Lourenço AH, Torres AL, Vasconcelos DP, Ribeiro-Machado C, Barbosa JN, Barbosa MA, Barrias CC, Ribeiro CC, Osteogenic, anti-osteoclastogenic and immunomodulatory properties of a strontium-releasing hybrid scaffold for bone repair, Materials Science and Engineering: C 99 (2019) 1289–1303. [PubMed: 30889663]

[86]. Silva GAB, Bertassoli BM, Sousa CA, Albergaria JD, de Paula RS, Jorge EC, Effects of strontium ranelate treatment on osteoblasts cultivated onto scaffolds of trabeculae bovine bone, Journal of bone and mineral metabolism 36(1) (2018) 73–86. [PubMed: 28321651]

[87]. Lino AB, McCarthy AD, Fernández JM, Evaluation of strontium-containing PCL-PDIPF scaffolds for bone tissue engineering: in vitro and in vivo studies, Annals of biomedical engineering 47(3) (2019) 902–912. [PubMed: 30560305]

[88]. De Witte T-M, Fratila-Apachitei LE, Zadpoor AA, Peppas NA, Bone tissue engineering via growth factor delivery: from scaffolds to complex matrices, Regenerative Biomaterials 5(4) (2018) 197–211. [PubMed: 30094059]

[89]. Goonoo N, Bhaw-Luximon A, Mimicking growth factors: role of small molecule scaffold additives in promoting tissue regeneration and repair, RSC Advances 9(32) (2019) 18124–18146.

[90]. Claire ES, Molly EO, Edward AB, Regulation of Angiogenesis and Bone Regeneration with Natural and Synthetic Small Molecules, Current Pharmaceutical Design 19(19) (2013) 3403–3419. [PubMed: 23432670]

[91]. Yu X, Khalil A, Dang PN, Alsberg E, Murphy WL, Multilayered Inorganic Microparticles for Tunable Dual Growth Factor Delivery, Advanced Functional Materials 24(20) (2014) 3082–3093. [PubMed: 25342948]

[92]. Dose Effect of Dual Delivery of Vascular Endothelial Growth Factor and Bone Morphogenetic Protein-2 on Bone Regeneration in a Rat Critical-Size Defect Model, Tissue Engineering Part A 15(9) (2009) 2347–2362. [PubMed: 19249918]

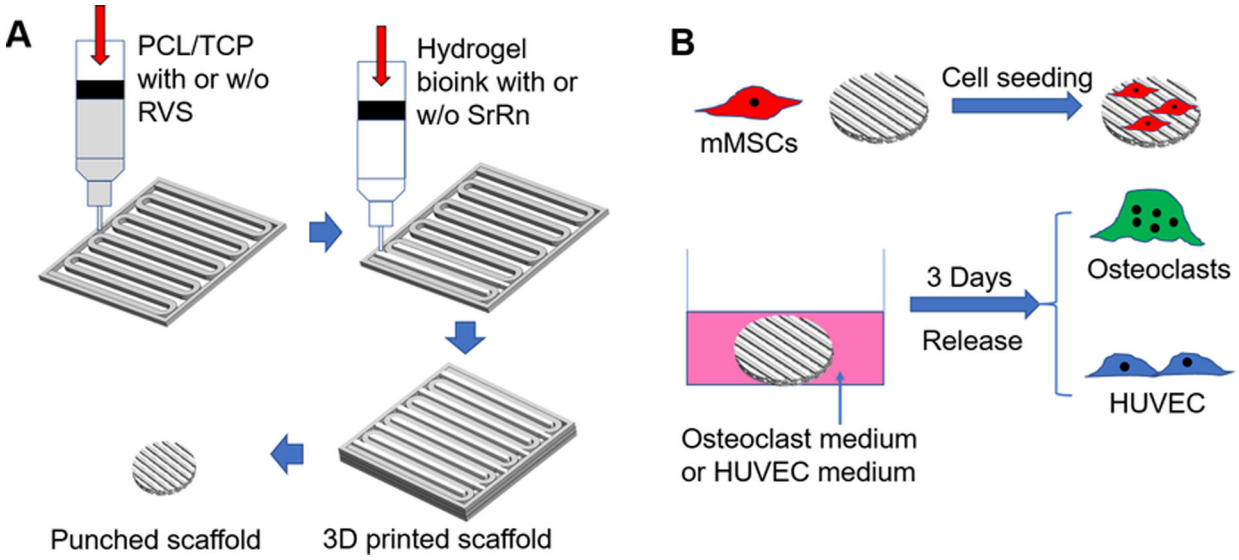

Figure 1.

(A) Schematic representation of the 3D printing of bone scaffolds incorporated with dual small molecules; (B) Overall *in vitro* experimental designs and methods.

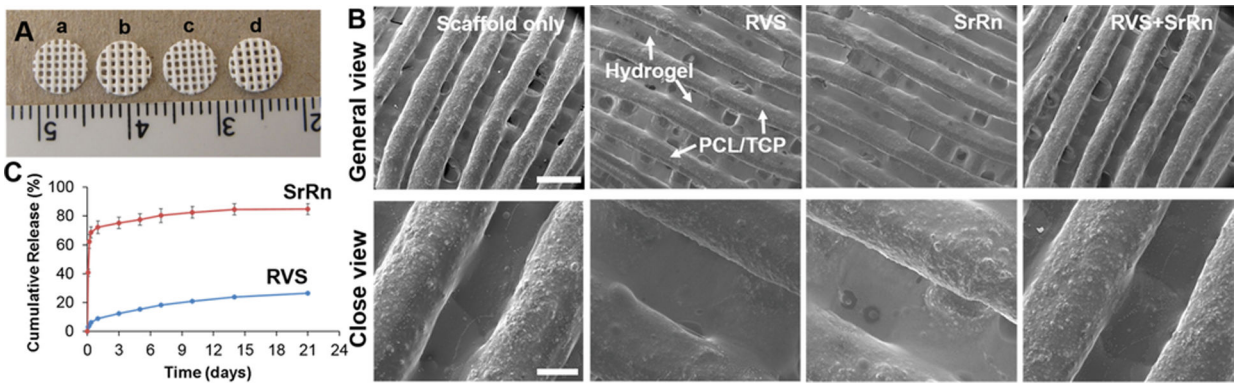

Figure 2.

Characterization of 3D printed scaffolds. (A) Representative images of different 3D printed scaffolds after punching: (a) scaffold only; (b) scaffold with RVS; (c) scaffold with SrRn; (d) scaffold with RVS+SrRn; (B) Typical SEM micrographs of 3D printed scaffolds with and without the incorporation of small molecules (scale bars: 1 mm for the general view and 300 μm for the close view); (C) Cumulative release of RVS and SrRn from 3D printed scaffolds after incubation in PBS at 37 °C.

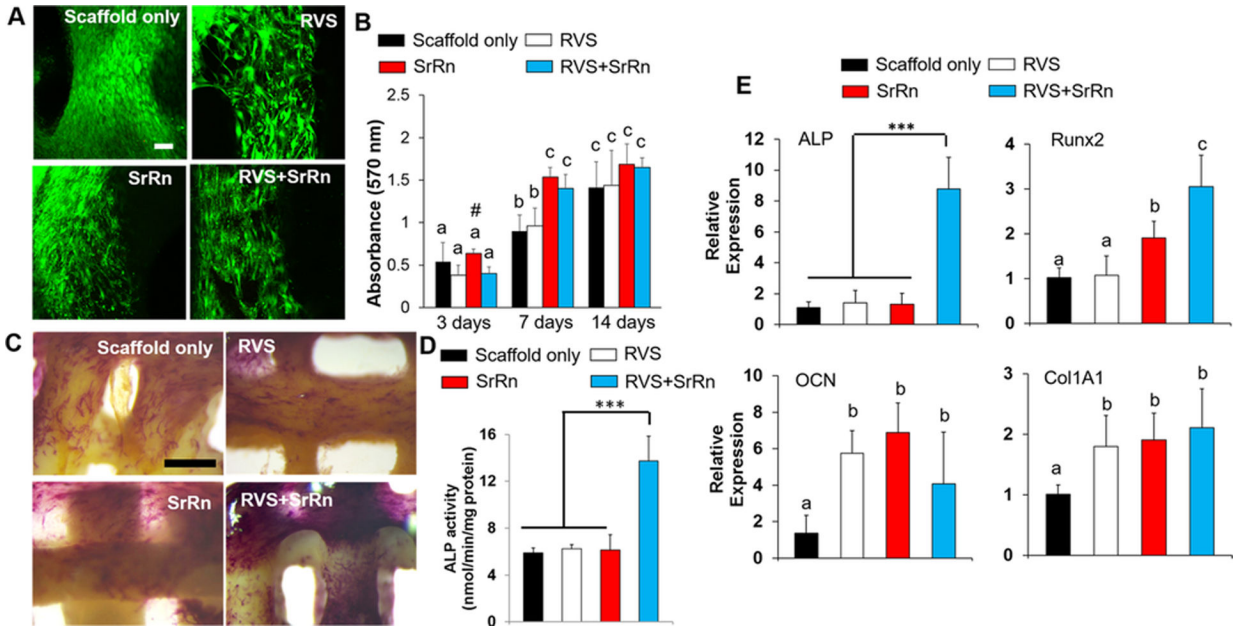

Figure 3.

Effects of 3D printed scaffolds, with and without the incorporation of small molecules, on mMSC viability, proliferation, and osteogenic differentiation. (A) Typical live/dead staining images (scale bars: 100 μm, red: dead cells, green: live cells) of mMSC on different scaffolds; (B) MTT assay for mMSC proliferation seeded on various scaffolds (n=5, bars that do not share letters are significantly different from each other (p<0.05), # indicates a significant difference compared to the scaffold only group); (C) ALP staining images of the various scaffolds with mMSCs after osteogenic induction (scale bars: 500 μm); (D) ALP activity test (n=5, ***p<0.001); (E) qPCR analysis of ALP, Runx2, OCN, and Col 1A1 genes for mMSC seeded on different scaffolds after 14 day differentiation (n=3; ***p < 0.001, bars that do not share letters are significantly different from each other (p<0.05)).

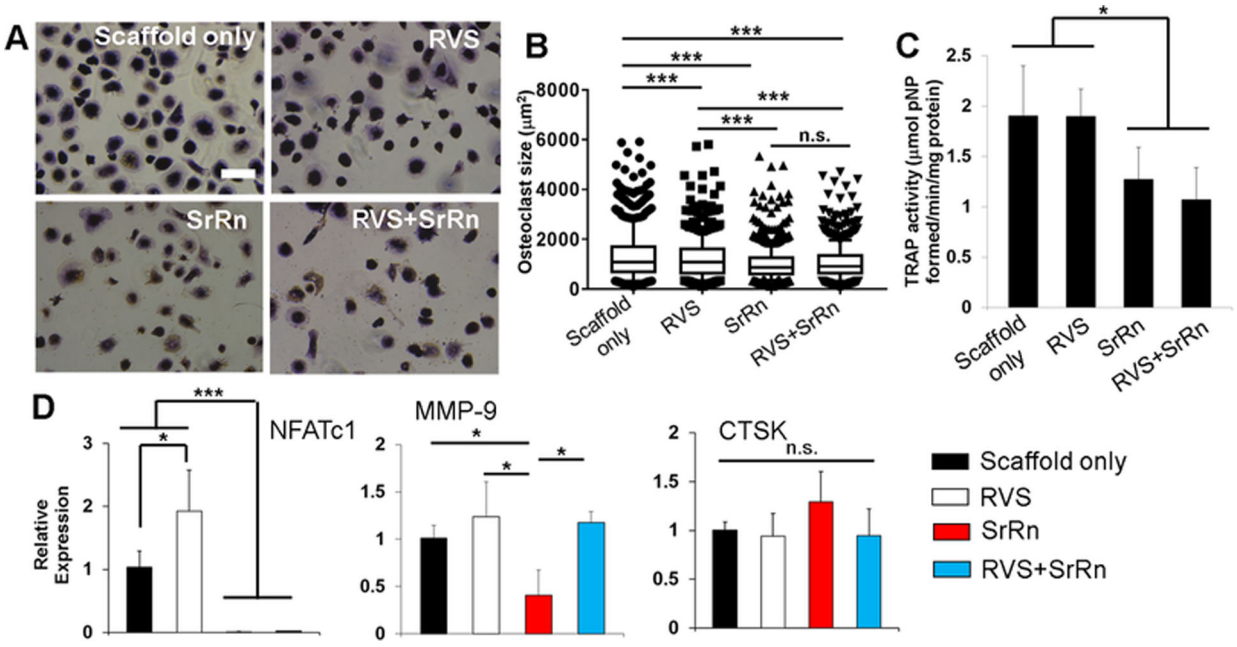

Figure 4.

Effects of released small molecules on human monocyte-derived osteoclast morphology, size, TRAP activity, and gene expression. (A) TRAP staining images of osteoclasts treated with released media with RVS and SrRn (scale bars: 200 μm); (B) Measurement of osteoclast size based on TRAP staining images (at least three images were taken from each samples, and 5 samples were used for each scaffold group; ***p<0.001, n.s. indicates no significant difference); (C) TRAP activity (*p<0.05); (D) qPCR analysis of NFATc1, MMP-9, and CTSK genes for osteoclasts (n=3; *p<0.05, ***p < 0.001).

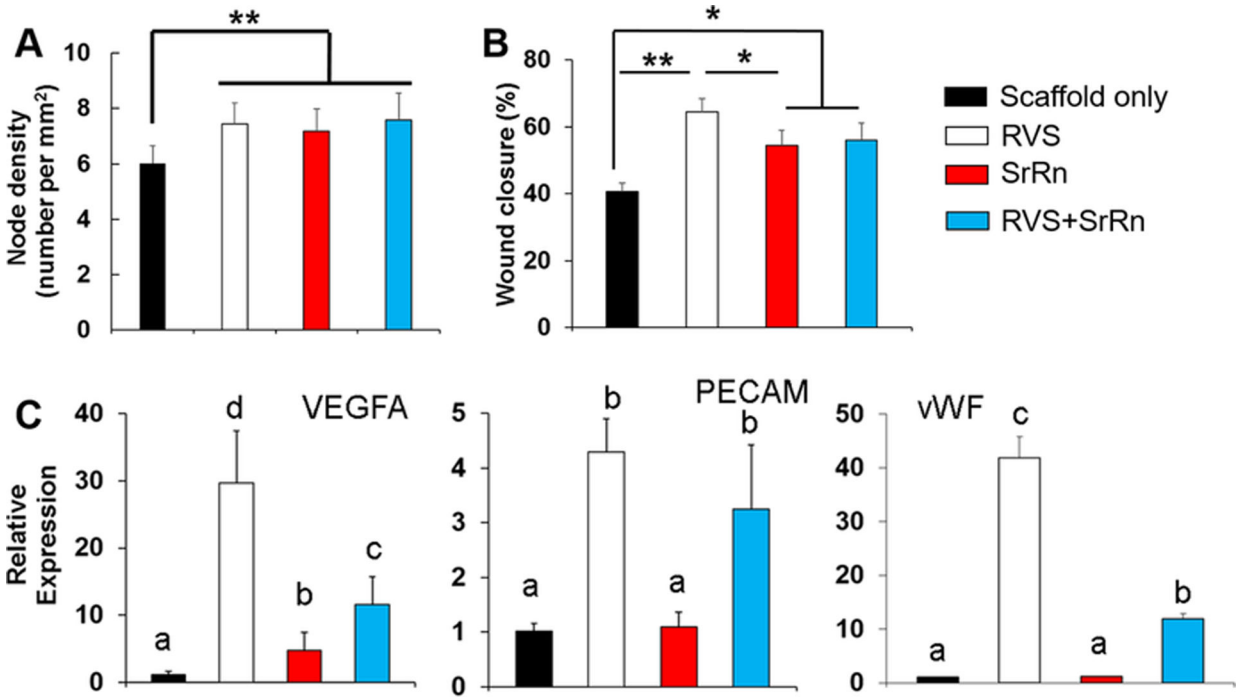

Figure 5.

Effects of released small molecules on HUVEC tube formation, migration, and gene expression. (A) Node density measured based on the formed tubes (n=4, $^{**}p<0.01$); (B) Wound closure percentage by measuring the distance of HUVEC migration in the wound scratch assay (n=4, $^{*}p<0.05$, $^{**}p<0.01$); (C) qPCR analysis of VEGFA, PECAM, and vWF genes for HUVEC (n=3; bars that do not share letters are significantly different from each other ($p<0.05$)).

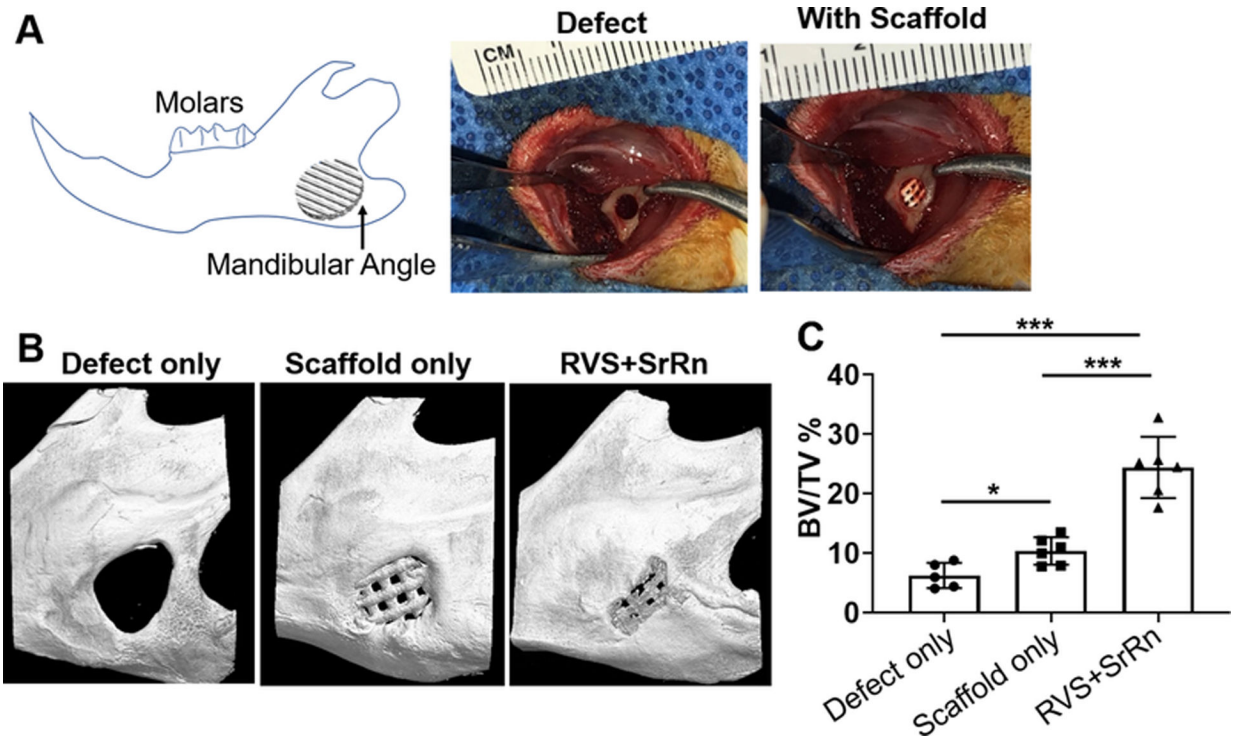

Figure 6.

Implantation of 3D printed scaffolds with and without small molecules into the rat model with critical-size mandibular defect. (A) Schematic drawing to show the implantation location; (B) Representative images of the animals with mandibular defects and with implantation of 3D printed scaffolds loaded with RVS and SrRn; (C) Representative micro CT reconstruction images at 8 weeks after surgery in different groups; (D) Micro CT quantification of bone volume to the total volume of the former defect area (BV/TV, n=5–6, *p<0.05, ***p<0.001).

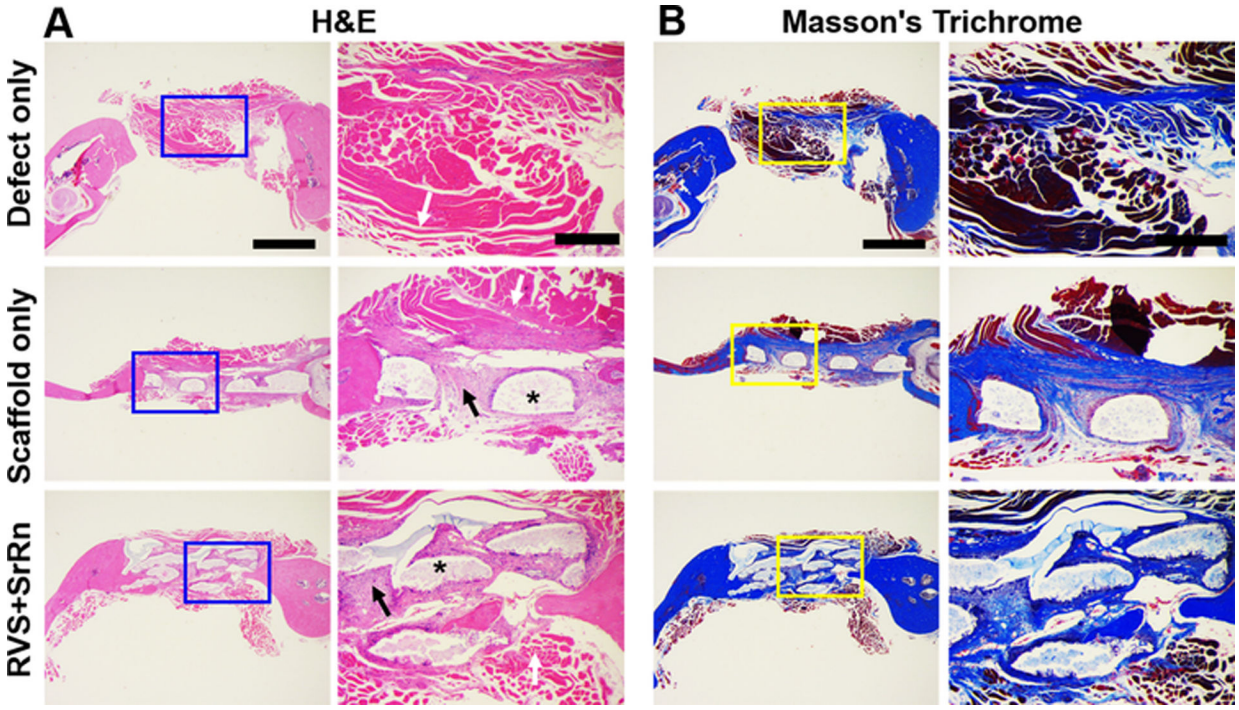

Figure 7.

Histological staining and observations of the newly formed bone in the three groups. (A) H&E staining; (B) Masson's Trichrome staining. Scale bar: 1 mm for general view, 400 μm for close view. White arrows indicate soft tissue, * indicate scaffolds, black arrows indicate newly formed bones.